Catalysis Letters, Vol. 118, Nos. 1–2, October 2007 (© 2007)
DOI: 10.1007/s10562-007-9138-1

Synthesis, characterization and hydroisomerization catalytic performance of nanosize SAPO-11 molecular sieves

Shengzhen Zhang, Sheng-Li Chen,* Peng Dong, Zhiyong Ji, Junying Zhao, and Keqi Xu

State Key Laboratory of Heavy Oil Processing, College of Chemistry and Chemical Engineering, China University of Petroleum, Beijing 102249, P. R. China

Received 15 April 2007; accepted 15 May 2007

A new static hydrothermal method was developed for synthesizing nanosize SAPO-11 molecular sieve.The new method involves aging pretreatment step followed by crystallization process of a precursor gel. The effect of the aging pretreatment on morphology and size of SAPO-11 molecular sieves was investigated. The results of XRD and SEM showed that the aging pretreatment changed the size and morphology of the SAPO-11 dramatically, and the size could be controlled by varying the time for aging. Nanocrystals of SAPO-11 molecular sieves were synthesized by aging the precursor gel at 150 °C for 135 min and then crystallizing the gel at 190 °C for 24 h. Compared with the SAPO-11 samples that exhibit the pseudo-spherical aggregates ranging from 3 to 15 μm synthesized by conventional method, the SAPO-11 samples synthesized by the new method not only possessed much smaller cubic single crystals of about 400–500 nm, but were more uniform in size. Moreover, the SAPO-11 samples synthesized by the new method had larger specific surface area and larger external specific surface area. The results of *n*−hexadecane hydroisomerization showed that the Pt/SAPO-11 prepared with the new method exhibited higher catalytic activity and better hydroisomerization selectivity than the Pt/SAPO-11 synthesized by conventional hydrothermal method.

KEY WORDS: aging treatment; hydroisomerization; nanocrystals; *n*−hexadecane; SAPO-11 molecular sieves; static hydrothermal synthesis.

1. Introduction

Silicoaluminophosphate molecular sieves denoted as SAPO were synthesized by Lok et al. [1] and composed of strictly alternating AlO_4, PO_4 and SiO_4 tetrahedra. Among of these SAPO materials, SAPO-11 has the AlPO4-11 (AEL) topology, comprising of unidirectional, non-intersecting, 10-membered ring channels with elliptical pore apertures of 0.39 nm × 0.63 nm. Recently, SAPO-11 has been found to be highly active and selective for the skeletal isomerization of *n*−butene [2], especially for the hydroisomerization of long-chain *n*−paraffins [3–5]. Owing to the medium acidity and suitable pore size of SAPO-11, Pd or Pt/SAPO-11 catalyst shows excellent performance in iso-dewaxing to produce high quality lubricant with low pour point and high viscosity index.

For long-chain *n*-paraffin, which is components of wax in petroleum products, the hydroconversion takes place mainly in the pore mouth and the external surface of the catalyst [6]. Thus, for the SAPO-11 used for hydroisomerization of heavy *n*−alkanes, only the active sites near pore mouths and on external surface are effective. In comparison with micrometer-sized zeolites, nanocrystalline SAPO-11 molecular sieves have large external surface and more pore mouths for hydroisomerization performance of long-chain *n*−alkane. Therefore, there is an increasing interest in the preparation and application of nanocrystalline-sized molecular sieves.

SAPO-11 molecular sieve is usually synthesized through traditional static hydrothermal crystallization at 160–220 °C using di-*n*-propylamine or/and di-*iso*-propylamine as structure-directing template, H_3PO_4 as source of P, pseudoboehmite as source of Al and silica sol or tetraethylorthosilicate (TEOS) as source of Si. The crystal morphology of SAPO-11 synthesized by the traditional hydrothermal method often exhibits pseudo-spherical aggregates of cubic plates ranging from 3 to 10 μm owing to the rapid congregativeness of crystal nuclei [7–9]. P. Meriaudeau et al. [10] and Q. Zh. Li et al [11] have been devoted to synthesizing the SAPO-11 molecular sieves using a two-liquid phase method, the synthesis medium of which involves aqueous phase, and non-miscible organic phase. However, beside the expensive cost, samples obtained by this method still exhibit pseudo-spherical aggregates ranging from 3 to 6 μm. How to synthesize nanometer-sized or submicron-sized SAPO-11 crystals has attracted a lot of attention of worldwide researchers.J. M. Su et al. [12] synthesized the SAPO-11 crystals with dimension between 500 and

*To whom correspondence should be addressed.
E-mail: slchen@cup.edu.cn

1000 nm using alcohol (such as isopropyl alcohol) as dispersing agent. The use of alcohol organics increases the preparing cost.

In this work, nanosize the SAPO-11 molecular sieves were synthesized by introducing an aging step into the procedures of conventional static hydrothermal method, without use of organic additives as dispersion agent. The synthesized SAPO-11 were characterized with XRD, FT-IR and SEM and the influence of aging conditions on the SAPO-11 was investigated. The catalytic performance of the SAPO-11 molecular sieves nanocrystals was evaluated through *n*–hexadecane hydroisomerization.

2. Experimental

2.1. Synthesis of SAPO-11 samples

The SAPO-11 samples were prepared as follows. First, pseudoboehmite (70 wt% Al_2O_3) was mixed with ortho-phosphoric acid (85 wt% H_3PO_4) and distilled water, stirred in a gelation vessel and heated in a water-bath at 35 °C for a while. Then, a mixture of *di-n*-propylamine (DPA) and *di-iso*-propylamine (DIPA) in a molar ratio of 6 to 4, used as template, and a fixed amount of silica sol suspension (25 wt% SiO_2) were added into the vessel. Later on, 3 M H_2SO_4 solution was used to adjust the pH value to 3.5–4.0. The molar composition of the reaction mixture was 1.0 P_2O_5:1.0Al_2O_3:0.4SiO_2: 1.0(DPA + DIPA). After that, the gel was transferred into a stainless-steel autoclave lined with polytetrafluorethylene (PTFE), and aged at 150 °C for some period of time with no stirring. The aged gel was cooled down, added with the fixed amount of distilled water and finally heated up to 190 °C for ~24 h for crystallization. The detailed procedure was described in ref [13].

For comparison, the synthesis of SAPO-11 with traditional hydrothermal technology was performed using the same molar composition and at the same condition without the aging step.

The as-synthized products were washed, centrifuged, filtrated, dried at 120 ° for 10 h, and then calcined at 600 °C for 24 h in air in order to remove the template. Pt/SAPO-11 bifunctional catalysts with 0.5 wt% Pt were prepared by impregnating the calcinated SAPO-11 samples with H_2PtCl_6 aqueous solution, drying them at 120 °C for 6 h and finally calcinating them at 350 °C for 3 h in air.

2.2. Characterization

Power X-ray diffraction patterns (XRD) were recorded on a SHIMADZU-6000 diffractometer, using the Cu$K\alpha$ (λ = 1.5404 Å) radiation at 40 kV and 30 mA with a scanning rate of 2 °/min. The morphology of the products was examined by a Cambridge S-360 scanning electron microscope (SEM). The composition of final materials were determined by sequential X-ray Fluorescence Spectrometer (SHIMADZU, XRF-1800).

The characterization of surface area and pore volume of the SAPO-11 molecular sieves was performed by using N_2 adsorption-desorption at −196 °C, in a Micromerities ASAP 2020 automatic adsorption apparatus. Samples were degassed at 350 °C for 3 h under a vacuum of 1.33×10^{-3} Pa prior to N_2 physisorption. The BET surface areas of the samples (A_{BET}) were calculated by applying the BET equation [14] to N_2 adsorption data in relative vapour pressure (p/p_0) range of 0.05–0.30. The cross-sectional area of N_2 molecule was taken as 16.20 $Å^2$. The pore volume (V_p) of the catalysts were obtained by extrapolating the upper parts of the desorption branches of the N_2 adsorption–desorption hysteresis loops to the relative pressure (p/p_0) of 1.0 [15]. The mean pore diameter (d) of the SAPO-11 molecular sieves were calculated with $d = 4Vp/A_{BET}$ assuming a cylindrical pore model. The pore size distributions in the pore diameter range of 1.5–100 nm of the samples were obtained by applying the expanded BJH equations [16] to the N_2 desorption branches of the hysteresis loops. Size distribution of microspores was determined by the HK method, and the external surface areas of the samples were calculated by the *t*-plot method [17].

The IR spectrum of the synthesized molecular sieves was recorded on a Nicolet Magna-IR 560 E.S.P. spectrometer in rang of 400–4000 cm^{-1} using KBr as reference. To avoid the effect of water, the samples were treated at 120 °C for 2 h.

2.3. Catalytic evaluation

Prior to the reaction, the catalysts were reduced in flowing hydrogen at 400 °C for 4 h. The hydroconversion of *n*-hexadecane were carried out in a continuous fixed-bed downstream reactor. The reaction conditions were as follows: H_2 pressure, 8 MPa; weight hourly space velocities (WHSV), 1.0–2.4 h^{-1}; H_2/n–C_{16} molar ratio, 10; and reaction temperature ranging from 330 to 370 K. The composition of products was analyzed by a SP3420 gas chromatography with a flame ionization detector (FID) and a capillary column OV-101 (50 m × 0.32 mm × 0.5 μm).

3. Results and discussion

3.1. Effect of aging step

Although zeolites crystallization under laboratory conditions is generally performed at elevated temperatures, it may be strongly influenced by the events taking place in the initial precursor system. Aging is a well-known process performed prior to the crystallization of zeolites; it can make the gel homogeneous. Meanwhile, some structural rearrangements might occur during aging that lead to the formation of zeolite nuclei [18–20].

In the present investigation, the change in the crystal phase and morphology of the gel during aging was studied.

The XRD patterns of the dried precursor gels obtained at period of aging of 0, 105, 135 and 180 min at 150 °C are shown in figure 1. The XRD results showed that in the initial period before 135 min, no characteristic peaks of SAPO-11 appeared, indicating that the precursor gel was still an amorphous. After 180 min of aging, the characteristic peaks of SAPO-11 between 20 and 23° became evident and sharp, indicating that SAPO-11 was formed and the crystals had grown large enough that XRD instrument could detect it. But at this time, the forming process for the pure SAPO-11 framework structure (XRD pattern is shown as figure 1(d)) was not complete, as a lamellar phase with an intense peak at about 6.1° was observed. The formation of similar precursor lamellar phase during the synthesis of $AlPO_4$s and SAPOs has already been reported [21]. The XRD pattern of the precursor gel aged for 135 min showed that there were some small and broad characteristic peaks at about 20–25°, implying that tiny nuclei of SAPO-11 accompanied by lamellar phase had formed at this stage.

Shown in figure 2 are the SEM of the dried precursor gels aged at 150 °C for 0, 105, 135 and 180 min. During the initial period of aging <135 min, no crystal obtained (as showed in figure 1(a) and (b)). This period may be ascribed to be the introduction period of the crystal nuclei. As the aging time increasing, the crystal nuclei were formed gradually. For the precursor gel aged 135 min, although some small characteristic peaks of SAPO-11 were detected (as shown in figure 1(c)), the grains were too tiny to be observed by SEM. As the aging process proceeded for 180 min., the SAPO-11 nuclei grown up.and then aggregated to form pseudo-spherical particles with a broad size distribution ranged in 3–10 μm (as shown in figure 2(d)).

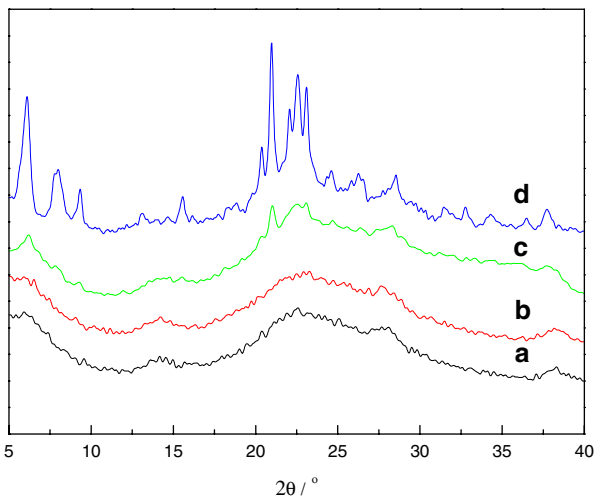

Figure 1. XRD spectra of precursor gels aged at 150 °C for (a) 0 min, (b) 105 min, (c) 135 min and (d) 180 min.

Infrared spectra of the aged precursor gels in the framework vibration frequency region are shown in figure 3. In general, the infrared spectrum of zeolite molecular sieves can be classified into two groups of vibration: (a) internal vibration of the framework TO_4 (T = Al, Si, P) including asymmetric stretch (ν_{asym}) at 1250–920 cm^{-1}, symmetric stretch (ν_{sym}) at 720–650 cm^{-1} and T–O (T = Al, Si, P) bend at 500–420 cm^{-1}, which are insensitive to structural vibration; (b) external linkage vibration of the TO_4 units in the structure including double ring at 650–500 cm^{-1}, asymmetric stretch at 1150–1050 cm^{-1}, symmetric stretch at 750–820 cm^{-1} and pores opening at 420–300 cm^{-1}, which are sensitive to structural variation [22]. The various vibration frequencies have been assigned [23,24].

In agreement with the XRD data, the infrared spectra displayed the gradual formation of SAPO-11 molecular sieves. In figure 3, the bands at 1400, 1474 and 1636 cm^{-1} detected during all the aging period are assigned to the C–H bending modes of the template. At the initial period of aging, i. e. aged for 0 min, some characteristic bands of amorphous phase were observed such as 619 and 525 cm^{-1}. With the aging time increasing, the bands of amorphous phase weakened. After the gel was aged for 105 min, the characteristic band of 4R (four-ring) was appeared at 627 cm^{-1}, implying that the secondary building units (SBU) had come into being that might be the unit of parent chain of some silicoaluminophosphate molecular sieves. At 135 min of aging, the characteristic bands of SAPO-11 (627, 587 and 550 cm^{-1}) appeared clearly, indicating that the nuclei of SAPO-11 molecular sieves were formed. The characterization absorbed bands of SAPO-11 sharpened as the aging process further proceeded, as shown in figure 3(d), implying that the SAPO-11 crystals weres growing up with time.

As a consequence, from the XRD, SEM and IR of the gel aged for different time, it was concluded that, the formation of SAPO-11 experienced such successive stages as gel condensation, formation of secondary structure units, formation of nuclei, and growth of crystals. Interruption to the aging process at different stages may influence the topology and morphology greatly of the final product.

3.2. Characterization

As shown in figure 4, the sample synthesized by conventional static hydrothermal method (sample S0) is different from the samples synthesized by improved method (samples S1–S3) in the topology and morphology, Pure SAPO-11 molecular sieves were synthesized by conventional static hydrothermal method and by the improved method with the precursor gel being aged for more than 135 min at 150 °C. However, if the aging time of the precursor gel was shorter than 135, e.g.,

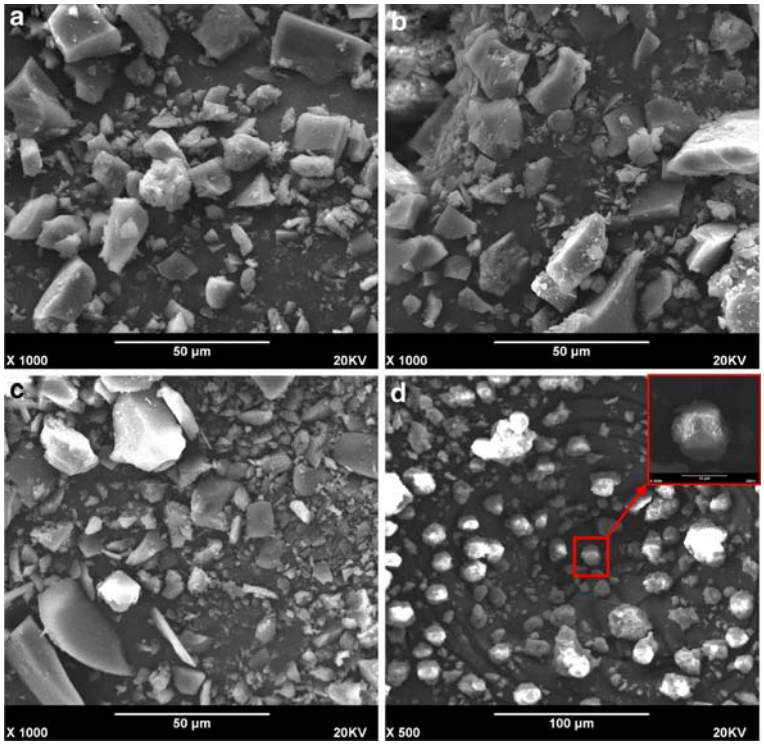

Figure 2. SEM of precursor gels aged at 150 °C for (a) 0 min, (b) 105 min, (c) 135 min and (d) 180 min.

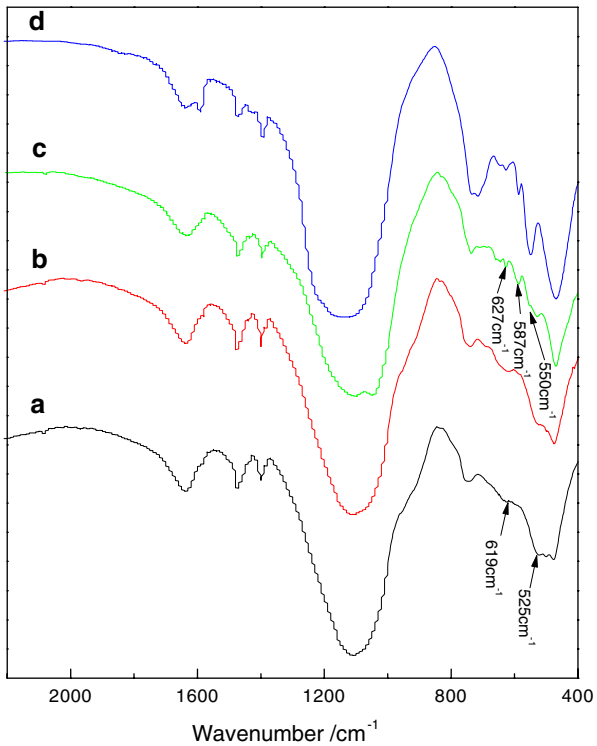

Figure 3. IR spectra of precursor gels aged at 150 °C for (a) 0 min, (b) 105 min, (c) 135 min and (d) 180 min.

105 min, the AlPO-C-Hydrated crystals [25] were obtained by the improved method. The SEM of samples synthesized from the improved method and the conventional method were shown in figure 5. The S0 sample synthesized from the conventional static hydrothermal method exhibited pseudo-spherical aggregates and got

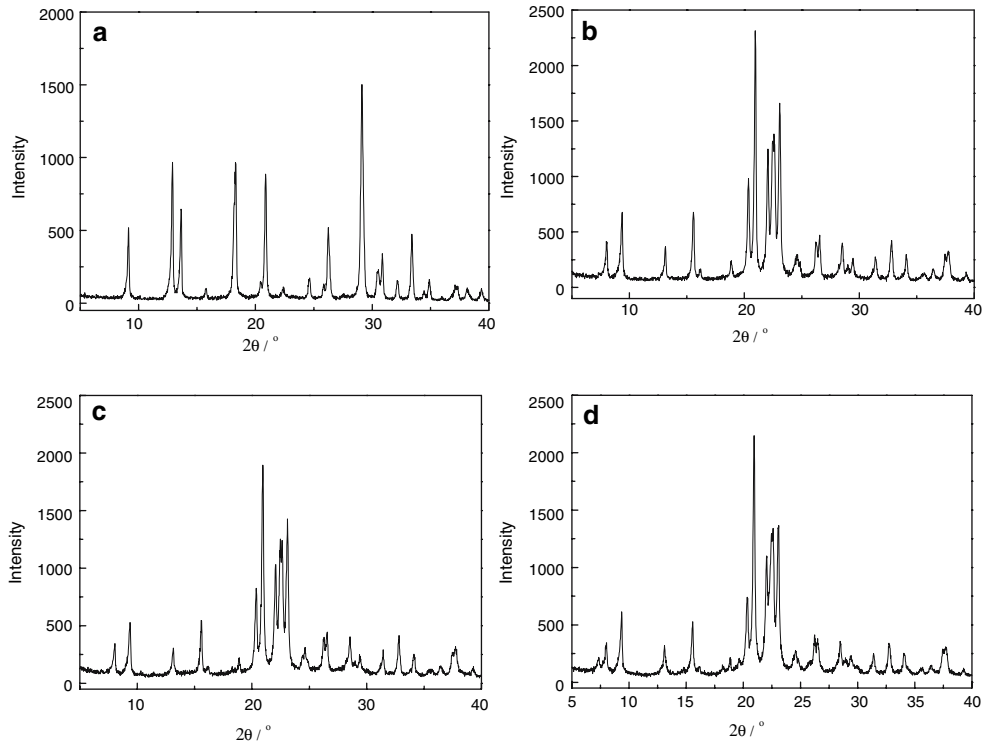

Figure 4. XRD patterns of samples synthesized by static hydrothermal method at 190 °C for 24 h from the precursor gels aged at 150 °C for (a) 105 min (S1), (b) 135 min (S2) and (c) 180 min (S3), and by (d) conventional method (S0).

the size ranging from 3 to 15 μm. The S1 sample synthesized from the improved method by aging the precursor gel at 150 °C for 105 min was fusiform crystals. However, when the aging time was prolonged to 135 min, the cubic SAPO-11 nanocrystals with uniform morphology and size about 400–500 nm were acquired as shown in figure 5(b). When the aging time was further prolonged to 180 min at 150 °C, the product was returned to the pseudo-spherical aggregates ranging from 7 to 15 μm (shown in figure 5(c)). The gel aging process was also performed at 130 and 175 °C for different time. The pure SAPO-11 molecular sieves could not be prepared until the precursor gel aging time was 210 and 100 min at 130 and 175 °C, respectively. Shown in figure 5(e) and (f) are the SEM of nanosize SAPO-11 samples prepared by the improved method, the aging temperature of which was 130 and 175 °C respectively. As a consequence, a suitable aging time at a given temperature is vital important for the synthesis of the nanosize SAPO-11.

Oliver *et al.* [26] reported that the crystallization of most aluminophosphates presumably follows a chain-to-layer transformation process. The parent chain structure $[AlP_2O_8H_2]^-$ was fabricated by four-ring during the initial period of aging in the liquid system, assembling a nucleus of specific topology in the presence of structure-directing agent. The chain species were sensitive to the composition of the liquid system and the condition of synthesis. They may not only be hydrolyzed in solution leading to the formation of other chain structure types but concentrated causing cross-linking and leading to a porous layer or open framework structure. In the conventional synthesis procedure, due to the sustained high temperature, the formed chain species rapidly condense, and assemble into the nuclei of SAPO-11, which grow and congregate into pseudo-spherical aggregates with nonuniform morphology and size ranging from 3 to 15 μm (as shown in figure 4(d) and 5(d)). When the gel was aged at 150 °C for 105 min, chain species may be formed during the aging process and then hydrolyzed in solution to produce the precursor chain structure for AlPO-C-Hydrated in the course of the cooldown process, so AlPO-C-Hydrated crystal phase and fusiform crystallines came into being as shown in figure 4(a) and 5(a). As the aging time prolonged to 135 min at 150 °C, the chain species condensed causing cross-linking and leading to the nuclei of SAPO-11 in solution. The succedent cooldown treatment hindered the formation and aggregation of the SAPO-11 nuclei and when bring the aged gel temperature to 190 °C, the formation of SAPO-11 nuclei occurred once more. Therefore, in compared with the conventional method, the improved method could resulted in more SAPO-11 nuclei, which in turn conduce small size of SAPO-11 particles, as shown in figure 4(b) and 5(b). When the gel aging is over-proceeded to some point (e.g over 180 min at 190 °C), much nuclei of SAPO-11 were formed and congregated into large

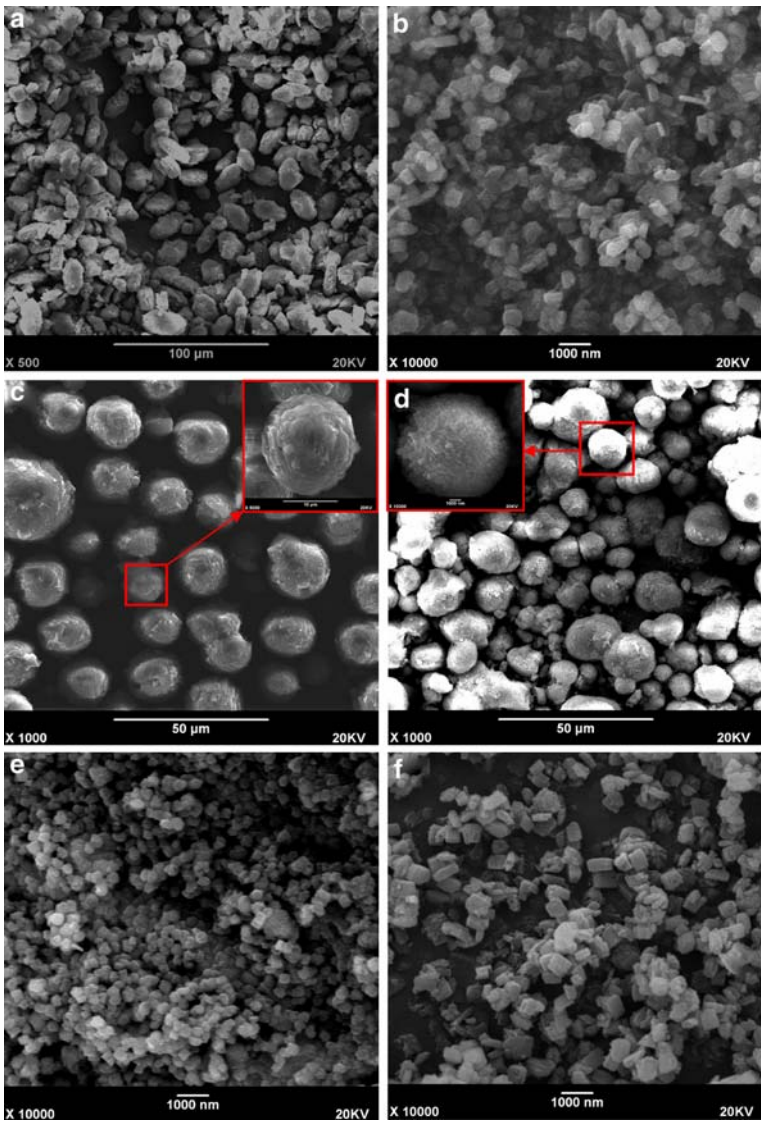

Figure 5. SEM micrographs of samples synthesized by static hydrothermal method at 190 °C for 24 h from the precursor gels aged at 150°C for (a) 105 min (S1), (b) 135 min (S2) and (c) 180 min (S3), (d) by conventional method (S0), (e) at 130 °C aged for 210 min (S4) and (f) at 175 °C aged for 100 min(S5).

spherical aggregates during the aging process (as shown in figure 2(d)). Therefore, it is impossible to synthesize nanosize SAPO-11 through nucleation of the over aged gel. The aging time not only effect the type of the formed molecule sieves, but also the size and morphology of the molecule sieves. Also the particle size was changed by the aging process of precursor gel, it is seems that the size of the single crystal of SAPO-11 kept constant, because the width of XRD peaks of these samples is almost unchanged, as shown in figure 4(b) and (d).

Listed in Table 1 are the chemical composition, the BET specific surface area, microporous surface area and the external surface area of the samples, synthesized by the conventional method and the improved method. The samples were synthesized from the precursor gel having the same compsotion as: $1.0P_2O_5$:$1.0Al_2O_3$:0.4-SiO_2:1.0(DPA + DIPA). The Si content of the S2 sample synthesized by the improved method was almost to that of the S0 sample prepared by conventional method. The SAPO-11 sample (S2) with small cubic single crystals synthesized by improved static hydrothermal method not only possesses larger BET surface area, but also has larger external surface area, which is calculated from isotherm using the *t*-plot method, than that of the S0 sample synthesized by the conventional static hydrothermal technology. Because the aggregation of SAPO-11 single crystals of S2 sample was hindered, S2 sample has more external surface area and pour mouths than that of sample S0, which was of large spherical aggregates (S0), while the microporous surface area of the two samples kept unchanged.

Table 1
Physicochemical properties of different SAPO-11 samples

Samples	Product composition	Specific surface area/m^2/g			Pore volume/cm^3/g	Pore diameter/nm
		S_{micro}[a]	S_{exter}[b]	S_{total}[c]		
S0	$(Al_{0.621}P_{0.330}Si_{0.049})O_2$	164.0	47.8	211.8	0.187	3.5
S2	$(Al_{0.650}P_{0.300}Si_{0.050})O_2$	152.6	89.6	242.2	0.196	3.3

[a]Microporous specific surface area(< 2 nm).
[b]External BET specific surface area.
[c]Total BET specific surface area.

A. Corma *et al.* [27] had ever synthesized SAPO-11 using organic–inorganic route in the presence of surfactant. The result had shown that the external surface area of the samples prepared with surfactant was much larger (ranged from 77 to 88 m^2/g) than that of the samples synthesized by conventional methods. But the microporous surface area of the samples obtained using surfactant was decreased by about a quarter and all the samples hold the similar total surface area *ca.* 175 m^2/g. Here in this work, the external surface area and the total surface area of SAPO-11 were increased without decreasing the microporous surface area through adding the aging process to the conventional method, without using a surfactant. Beside the good characteristics of the prepared SAPO-11, the organic-agent free method is more economical than those adopted by previous researchers.

3.3. Catalytic activity

The Pt/SAPO-11 catalysts were prepared by impregnating the SAPO-11 with solution of H_2PtCl_6.The amount of Pt loaded on the SAPO-11 was 0.5 wt% for all the prepared catalysts. M. Höchtl *et al.* [28] reported that 0.5 wt% of Pt loaded by the impregnation method could provide sufficient metal sites to match with the acid sites. The hydromerization of *n*-hexadecane were carried out in a continuous fixed-bed downstream reactor using the prepared Pt/SAPO-11 as catalyst. The conversion of *n*-hexadecane and the selectivity for *iso*-hexadecane as function of weight hourly space velocity and temperature are shown in figure 6 and 7, respectively. The conversion of *n*-hexadecane increased with the reaction temperature and decreased with the space velocity, while the selectivity decreased with the reaction temperature and increased with the space velocity. It is obvious that, at the same reaction conditions, both the conversion and the selectivity over Pt/S2 catalyst are much greater than those over Pt/S0 catalyst in all range of reaction temperature and space velocity.

For the hydroisomerization of long chain *n*-alkane over the 10-ring tubular pore molecular sieve catalysts, such as ZSM-22 and SAPO-11, the reaction and adsorption took place on the external surface of crystals and on the pore mouths [6,29,30]. The greater activity obtained with SAPO-11 nanocrystals can be explained by their smaller crystals size. For the mechanism of long-chain alkanes hydroisomerization over bifunctional catalyst, if there are enough hydrogenating sites, the rate determining steps are assured to be carbenium rearrangement over acid supporters. The larger number of active sites of supporters possess, the greater will be the conversion of long chain alkanes. Compared with S0 sample synthesized by conventional method, S2 sample possessed larger external surface area and smaller particle's size, which provide more accessible pore mouths and more active sites, leading to its greater catalytic activity. Besides, reduction in crystalline size of the molecular sieves can decrease the diffusion length and then significantly increase the diffusion rate of reactants inside the SAPO-11 particles, resulting in high catalytic activity of the catalysts [31].

As shown in figure 6 and 7, within the range of weight hourly space velocity and the reaction temperature, the catalyst Pt/S2 give higher hydroisomerization selectivity than the catalyst Pt/S0. The better isomerization performance of catalyst Pt/S2 is due to the smaller particle size of the SAPO-11 molecular sieves support. It is generally accepted that n-hexadecane will be dehydrogenated and then transformed, on Pt/SAPO-11 catalyst, into carbenium which can rearrange over pore mouth active sites to produce isomers of hexadecane or hydrocracking product. On the S2 catalyst with small particle size, the isomeric intermediates diffuse out of then the depart from the catalyst particles easily, so can suppress the hydrocracking reaction to some extent. Therefore, higher selectivity to *iso*-hexadecane over these catalysts can be achieved. As a contrast, it is difficult for the diffusion of monobranched isomer intermediates to diffuse out of the sample S0 with larger crystal size, so that the monobranched isomer intermediates has more opportunity to isomerize further into multibranched isomers which can be cracked more easily.

4. Conclusions

The aging pretreatment of the precursor gel in the preparation of SAPO-11 changed the crystal type, the size and the crystals morphology of SAPO-11. Aging the precursor gel at 150 °C for 135 min before the crystal-

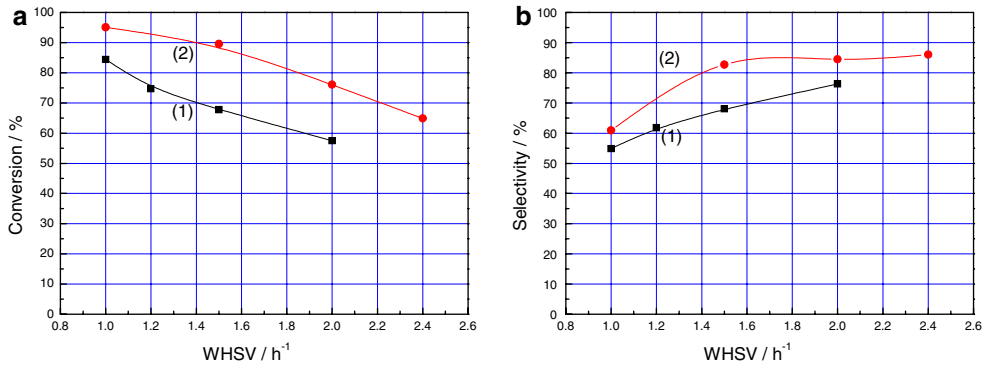

Figure 6. Catalytic performance of Pt/SAPO-11 catalysts at different space velocities during *n*-hexadecane hydroisomerization process (a) Conversion of *n*-hexadecane as a function of weight hourly space velocity; (b) Selectivity of *iso*-hexadecane as a function of weight hourly space velocity. (1) SAPO-11 supporter S0 prepared by the conventional method; (2) SAPO-11 supporter S2 prepared by the improved method. (Reaction conditions: 340 °C, 8 MPa, n_{H2}/n_{HC} 15).

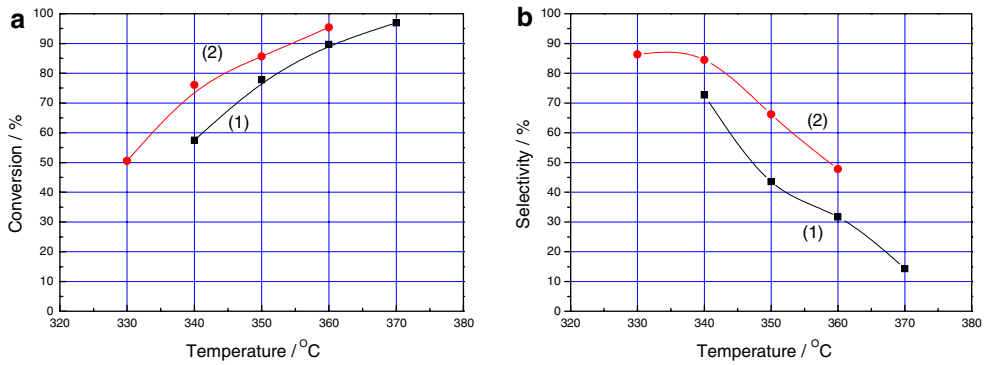

Figure 7. Catalytic performance of Pt/SAPO-11 catalysts at different reaction temperatures during *n*- hexadecane hydroisomerization process (a) Conversion of *n*- hexadecane as a function of reaction temperature; (b) Selectivity of *iso*- hexadecane as a function of reaction temperature. (1) SAPO-11 supporter S0 prepared by the conventional method; (2) SAPO-11 supporter S2 prepared by the improved method (Reaction conditions: 8 MPa, n_{H2}/n_{HC} 15, WHSV 2.0 h^{-1}).

lization process can synthesize more uniform zeolite particles with size about 400–500 nm, much smaller than those synthesized by conventional method with spherical aggregates diameter ranged from 3 to 15 μm. Compared with the sample synthesized by conventional method, the nanosize SAPO-11 prepared by the improved method exhibited not only large external surface area and total surface area, but also great hydroisomerization activity and selectivity. The improved method is promising for the commercial manufacture of nanosize SAPO-11, which is useful in the hydroisomerization of long chain *n*-alkanes to produce low pour point diesel fuel and high-quality lubricant base oil.

References

[1] B.M. Lok, C.A. Messina, R.L. Patton, R.T. Gajek, T.R. Cannan and E.M. Flanigen. US. Patent 4, 440 (1984) 871.
[2] C.M. Lopez, F.J. Machado, J. Goldwasser, B. Mendez and K. Rodriguez, Zeolites 19 (1997) 133.
[3] M.J. Girgis and Y.P. Tsao, Ind. Eng. Chem. Res. 35(2) (1996) 386.
[4] J.M. Campelo, F. Lafont and J.M. Marinas, Appl. Catal. A 170 (1998) 139.
[5] K.C. Park and S.K. Ihm, Appl. Catal. A 203 (2000) 201.
[6] M.C. Cloaude and J.A. Martens, J. Catal. 190 (2000) 39.
[7] P. Meriaudeau, V.A. Tuan, V.T. Nghiem, S.Y. Lai, L.N. Hung-Caccache and C. Caccache, J. Catal. 169 (1997) 55.
[8] J.M. Campelo, F. Lafont and J.M. Marinas, Zeolites 15 (1995) 97.
[9] M. Alfonzo, J. Goldwasser, C.M. López, F.J. Machado, M. Matjushin and B. Méndez, J. Mol. Catal. A 98 (1995) 35.
[10] P. Mériaudeau, V.A. Tuan, F. Lefebvre, V.T. Nghiem and C. Naccache, Microporous Mesoporous Mater. 22 (1998) 435.
[11] X.D. Huang, L.J. Wang, L.D. Kong and Q. Zh. Li, Appl. Catal. A 253 (2003) 461.
[12] J.M. Su, J.W. Da, L.P. Wu, L.J. Jin, W.B. Liu and J.L. Liu, CN 1356264A (2002).
[13] Sh.L. Chen, Sh.Zh. Zhang, P. Dong CN 200610165510x (2006).
[14] S. Brunauer, P.H. Emmett and E. Teller, J. Am. Chem. Soc. 60 (1938) 309.
[15] H.E. Ries, W.G. Frankenburg and V.I. Komaarewsky, in: *Advances in Catalysis and Related Materials*, Vol. 4, (Academic Press, New York, 1952), 87 pp.
[16] S. Khaja Mastan, K.S. Rama Rao, P.S. Sai Prasad and P. Kanta Rao, Adsorp. Sci. Technol. 9 (1992) 212.
[17] J.M. Thomas and W.J. Thomas, in: *Principles and Practice of Heterogeneous Catalysis*, (VCH Publishers Inc., New York, 1997), Chap. 2.

[18] R.M. Barrer, in: *The Hydrothermal Chemistry of Zeolites*, (Academic Press: London, 1982), Chap. 4.
[19] L. Gora, K. Streletzky, R.W. Thompson and G.D. Phillies, Zeolites 18 (1997) 119.
[20] C.S. Cundy, J.O. Forrest and R.J. Plaisted, Stud. Surf. Sci. Catal. 135 (2001) 143.
[21] N. Venkatathri, S.G. Hegde, V. Ramaswamy and S. Sivasanker, Microporous Mesoporous Mater. 23 (1998) 277.
[22] R.R. Xu and W.Q. Pang, in: *Chemistry-Zeolites and Porous Materials*, (Scientific Press: Beijing, 2004), Chap. 3.
[23] J. Tuan, Zh.M. Liu, X.H. Bao, X.Ch. Liu, X.W. Han, Ch.Q. He and R.Sh. Zhai, Microporous Mesoporous Mater. 53 (2002) 97.
[24] M.H. Um and M.S. Kang, J. Ind. Eng. Chem. 11 (2005) 540.
[25] M.M.J. Treacy and J.B. Higgins, in: *Collection of Simulated XRD Powder Patterns for Zeolites* (Fourth Revised Edition), (Elsevier: Amsterdam, 2001), 54 pp.
[26] S. Oliver, A. Kuperman and G.A. Ozin, Angew. Chem. Int. Ed. 37 (1998) 173.
[27] T. Blasco, A. Chica, A. Corma, W.J. Murphy, J. Agúndez-Rodríguez and J. Pérez-Pariente, J. Catal. 242 (2006) 153.
[28] M. Höchtl, A. Jentys and H. Vinek, J. Catal. 190 (2000) 419.
[29] P. Mréiaudeau, Vu.A. Tuan, G. Sapaly, Vu.T. Nghiem and C. Naccache, Catal. Today 49 (1999) 285.
[30] J.A. Martens, G. Vanbutsele, P.A. Jacobs, J. Denayer, R. Ocakoglu, G. Baron, J.A. Muñoz Arroyo, J. Thybaut and G.B. Marin, Catal. Today 65 (2001) 111.
[31] Zh.M. Wang, Zh.J. Tian, F. Teng, G.D. Wen, Y.P. Xu, Zh.Sh. Xu and L.W. Lin, Catal. Lett. 103 (2005) 109.